



Evaluation of a diffuse interface treatment for pressure in phase change simulations using adaptive mesh refinement

Bernardo Alan de Freitas Duarte¹ · Millena Martins Villar¹ · Ricardo Serfaty² · Aristeu da Silveira Neto¹

Received: 11 September 2018 / Accepted: 8 January 2019 / Published online: 18 January 2019
© The Brazilian Society of Mechanical Sciences and Engineering 2019

Abstract

Phase change computational simulations using a diffuse interface treatment for pressure were investigated in order to quantify the spurious currents and its consequences on the interface transport in the present paper. In addition, benchmarks were conducted with a sharp interface treatment for pressure. Namely, a Delta function method (Delta) was employed for the diffuse interface treatment and a ghost fluid method (GFM) for the sharp approach. An additional force term in the non-divergent form of the momentum equation is proposed for the first time in the literature, and its impact on interface motion during simulations of bubble growth by intense phase change has been quantified. In addition, the influence of recoil force on interface position was evaluated in simulations of water bubble condensation at near critical pressure. Finally, simulations of a complex industrial application were performed using the diffuse interface treatment, namely a case of film boiling with the development of Rayleigh–Taylor instability. Both interface treatments presented excellent results for the interface evolution in time. Even with the presence of some relevant spurious currents in the Delta method, the bubble evolution in time was accurately predicted. The sharp interface treatment potential was especially evident using a mass density flux of $1.0 \text{ kg}/(\text{m}^2 \text{ s})$ or higher. Therefore, a diffuse interface treatment for pressure has been presented as an appropriate strategy for most phase change simulations since the presence of the spurious currents did not disturb the interface position, and its magnitude was low for even moderate phase change intensities. The inclusion of the source term due to the additional force in the non-divergent form of the momentum equation and the recoil force term was irrelevant in the cases tested. Lastly, the film boiling simulation using the diffuse interface treatment revealed the possibility of treating complex 3D cases for industrial applications with this method.

Keywords GFM method · Delta function method · Boiling · Spurious currents · Recoil force

1 Introduction

1.1 Original contributions of the present paper

A diffuse interface treatment for pressure generally produces spurious currents due to its numerical fundamentals; however, quantitative investigations of spurious currents and its implications for phase change simulations are scarce in the literature. In the present paper, the results of simulations

of bubble growth by phase change using a diffuse interface treatment for pressure were investigated in order to quantify the spurious currents and its consequences on the interface transport. In addition, benchmarks were conducted with a sharp interface treatment for pressure. An additional force term in the non-divergent form of the momentum equation was proposed for the first time in the literature, and its impact on interface motion during simulations of bubble growth by intense phase change has been quantified. In addition, the influence of recoil force on interface position was evaluated in simulations of water bubble condensation at near critical pressure. Finally, simulations of a complex industrial application were performed using the diffuse interface treatment, namely a case of film boiling with the development of Rayleigh–Taylor instability.

Technical Editor: Francis HR Franca, Ph.D.

✉ Bernardo Alan de Freitas Duarte
be1988aqua@gmail.com

¹ Federal University of Uberlândia, 2121 Av. João Naves de Ávila, Uberlândia, Brazil

² CENPES, Av. 1, Ilha do Fundão, Brazil

1.2 Organization of the present paper

The goal of the present paper is to report a quantitative analysis of some particular numerical aspects of phase change simulations using a diffuse interface approach for pressure.

Several classical phase change problems are numerically investigated in the present paper using a diffuse interface method in order to evaluate its characteristics and consequences. Spurious currents are quantified and compared to a sharp interface method for pressure. A validation case of bubble growth by constant phase change intensity is presented. Subsequently, a validation case of bubble growth by variable phase change intensity is studied. Then, an analysis of the effects from some additional forces in phase change problems is quantified and discussed. Next, the results of numerical simulations with three different intensities of phase change are given and the spurious currents quantified, along with a discussion of the results. The efficiency of the adaptive mesh refinement (AMR) method is evaluated using a correlation from the literature, and the results are compared to previous work on phase change. Lastly, the results of simulations of film boiling are presented, the efficiency of the AMR is evaluated, and both are compared to previous results in the literature. Some conclusions are drawn at the end of the paper, based on the results obtained in all the cases simulated.

1.3 Computational simulations of phase change

Phase change is an important issue in industrial applications [1] since it plays a critical role in a large number of processes [2, 3]. Boiling, for example, is a highly efficient way to transfer thermal energy, notably in industrial thermal exchangers [4]. Moreover, chemical separation techniques, such as distillation, are characterized by simultaneous mass and energy transfer [1]. Droplet evaporation is another phenomenon of indubitable importance, of great importance for certain applications [5], particularly burning liquid fuels. The earliest phase change numerical investigations in the literature presented important aspects of mathematical and numerical modeling, which can be seen in [3] and [2]. Later, several advances in mathematical and numerical modeling were achieved and reported in the literature with even complex simulations for industrial applications [6].

Numerical simulations of phase change are relevant to collecting information about flow characteristics since experiments dealing with phase change are usually difficult to be conducted correctly [7] due to the small spatial scales [2] and the rapidity of the phase change process [3].

Phase change simulations present several numerical obstacles [8]. One of the most challenging aspects is notably the discontinuities in the physical properties, occurring at the interface between the two fluids [9]. In addition, the jump conditions across an interface for properties such as pressure represent an important aspect to be considered in phase change simulations [6].

In order to impose jump conditions at the interface, a sharp or diffuse interface treatment can be used for each fluid variable. Sharp interface treatments usually provide an accurate definition of a fluid variable across the interface, improving the resolution of the jump condition [10]. The results from a diffuse interface treatment generally give a poor representation of the jump conditions at the interface since the fluid properties are smoothed across the boundary between the two fluids [6]. The development in the velocity field of spurious currents at the interface is a typical consequence of the employment of a diffuse interface treatment for pressure.

Fictitious velocities emerge due to an erroneous estimate of the surface tension force [11] and pressure gradient, depending on the numerical scheme employed [12]. In addition, the spurious currents tend to be intensified in phase change problems [6], and so they should be especially controlled in these numerical simulations. The spurious currents generally appear close to the interface when computations of a static bubble or droplet are performed with a diffuse interface treatment for pressure due to the surface tension force calculation [13]. According to Tanguy et al. [6], the intensity of the spurious currents increases when phase change occurs, due to the jump condition on the velocity field. In addition, the presence of spurious currents may be partly responsible for an inaccurate evolution in time of the interface, since this boundary's advection is performed using the local velocity field.

Tanguy et al. [6] have presented inaccurate results for a diffuse interface treatment in phase change simulations. Other works in the literature using a diffuse interface treatment, such as Samkhaniani and Ansari [14] and Lee et al. [15], have found numerical results with a low deviation with the literature. More studies are necessary to understand the consequences of using a diffuse interface treatment instead of a sharp strategy for one or more fluid variables in phase change simulations. In addition, it is appropriate to quantify these fictitious velocity fields in the phase change simulations in order to evaluate their consequences and to visualize the behavior of the motion of the interface in time to confirm the accuracy of the numerical model employed.

An investigation of a diffuse and sharp interface treatment for pressure in phase change simulations is conducted in the present paper, with the intent of quantifying the error and the effects found in the simulations using a diffuse and sharp approach for a pressure jump condition, evaluating the

performance of both interface treatments. A benchmark will be presented, and simulations with adaptive mesh refinement (AMR) will be compared to uniform grid simulations. In order to quantify the accuracy of each numerical strategy, the spurious currents and interface motion are evaluated.

The physical model used in the present study consists of a three-dimensional domain where the flow is considered incompressible and the fluids monocomponent. Lastly, simulations using the diffuse interface treatment for pressure were performed for a film boiling application to show the potential of the diffuse interface methodology to model even complex problems.

1.4 Jump conditions in phase change simulations

The literature presents two numerical strategies to impose jump conditions of fluid variables across the interface, namely the whole domain formulation and the jump condition formulation [6]. The whole domain formulation uses a Delta function method (Delta), in which the jump conditions are smoothed around the interface, smearing out discontinuous terms. The jump condition formulation uses a ghost fluid method (GFM) in which the interface is treated imposing the jump conditions by ghost cells [6, 10].

The Delta method computes the surface tension force using a continuum surface force (CSF) model [16] which usually generates spurious currents due to a numerical imbalance between the pressure gradient and the related surface tension force [13]. Even though the presence of spurious currents has been extensively observed by researchers since the inception of the CSF, to date there has been little quantitative analysis of their importance [11], especially when applied to problems involving phase change. Numerous approaches have been proposed to suppress spurious currents. Nevertheless, several methods have difficulty avoiding inducing unphysical flows, due to the numerical error in estimating the interfacial surface tension [7]. In contrast, the GFM approach computes the surface tension force without a smooth transition due to a sharp jump condition for pressure at the interface [13].

1.5 Particular forces in phase change problems

Two forces have been evaluated in the present work in order to better understand the importance and consequences of modeling them in phase change problems, namely the recoil force and the additional force due to the use of the non-divergent form of the momentum equation. For the first time in the literature of phase change, the additional force due to the use of the non-divergent form of the momentum equation is presented and quantified. The need for this additional term in phase change problems is reserved to the use of the non-divergent form of the momentum equation and the

occurrence of mass transfer at the interface. Since the interface cells do not present null-divergence velocity in phase change problems, the non-divergent form of the momentum equation naturally receives an additional term from the continuity equation. The details of this extra force term are described in the mathematical model section; later, the computational results section presents a quantitative analysis of the additional force term in phase change simulations.

During phase change, a recoil force appears at the interface between the two fluids due to changes in volume [17]. The intensity of the recoil force depends on the mass density flux occurring at the interface. The recoil force may be defined by [4]

$$\mathbf{f}_{\text{recoil}} = \dot{m}''^2 \left(\frac{1}{\rho_v} - \frac{1}{\rho_l} \right) \mathbf{n} \quad (1)$$

where \dot{m}'' is the mass density flux (this term is described in the mathematical model section), ρ is the specific mass, and \mathbf{n} is the normal vector.

The study of the recoil force in CFD investigations began 30 years ago [17]; however, few numerical investigations have dealt with phase change and quantified or evaluated the role and the importance of this force in the momentum equation. The term which models the influence of the recoil force is included in several publications in the literature, such as [15] and [6], although it is not even cited in other works, such as [2] and [12]. Up to now, only a few works have studied the influence of the recoil force in phase change problems, e.g., Raghupathi et al. [17]. The relevance of this term has been ignored in much of the phase change literature, and at the same time, it has been included in numerous numerical works without an evaluation of its importance or influence. An understanding of the significance of the recoil force in phase change problems may be important for understanding the underlying mechanisms behind the phase change fundamentals. Therefore, in the present paper, numerical simulations are investigated so as to compute the magnitude of this force and its importance in phase change problems.

1.6 Adaptive mesh refinement (AMR) in phase change problems

It is known that an accurate numerical solution of a partial differential equation relies on the discretization with a computational grid with sufficiently high resolution. On the other hand, simulations using uniform grids overly increase the computational costs due to the unnecessary refinement of a large region of the domain. A uniform and fine grid is generally associated with a high computational cost, which may impair its applicability to solving several complex problems of interest. In contrast, the AMR method is a computational

tool allowing the definition of criteria to guide a spatially non-uniform mesh refinement according to an indicator function, such as vorticity, temperature gradient or the presence of an interface.

AMR may provide a strategy for solving complex problems using less computational resources compared to uniform grids [12], and reducing the computational power requirement without affecting the precision of the numerical results [18]. The interest in using AMR in multiphase flows is particularly large since the interface region frequently requires fine grids due to the calculation of high gradients, whereas the rest of the domain usually does not require fine grids [19].

Recently, the AMR strategy for modeling some large-scale or complex problems has been employed in the phase change literature. In the present paper, the refinement criterion has been related to the interface location, as does most of the phase change literature, such as Akhtar and Kleis [12]. In order to make a quantitative evaluation of the improvement in terms of time and computational power attained by using AMR compared to uniform grids, a measure of the efficiency of the AMR is used to quantify the enhancement due to AMR strategy.

2 Mathematical model

Two topics are presented in the mathematical model section: the general equations related to the phase change phenomenon, and the mathematical details of the additional term in the momentum equation which is pertinent to phase change problems when using the non-divergent formulation.

2.1 Description of the general mathematical formulation

The mathematical formulation was employed in the non-divergent form as recommended by Deen and Kuipers [20]. Putting ρCp inside the substantial derivative would lead to a non-physical change of the enthalpy if the two materials next to each other present the same temperature but different ρCp , as demonstrated by Deen and Kuipers [20]. Therefore, the non-divergent form was used in the numerical simulations in order to avoid non-physical issues.

In order to compute the amount of phase change occurring at the interface, the present model uses the calculation of the mass density flux (\dot{m}''). The mass density flux is included in the mathematical formulation using source terms in the continuity and energy equations, and is defined by the following expression [6]:

$$\dot{m}'' = \frac{k_1 \nabla T_1 \cdot \mathbf{n} - k_v \nabla T_v \cdot \mathbf{n}}{L} \tag{2}$$

where k is the thermal conductivity, L is the latent energy, T is the temperature, and \mathbf{n} is the normal vector.

Phase change problems present null velocity divergence in the bulk of each phase, and at the interface, there is a source term for mass balance [3]. The continuity equation is expressed using a Dirac Delta function in the right-hand side to take into account the source term only over the interface, according to the following equation [6]:

$$\nabla \cdot \mathbf{v} = \int_{\Gamma} \left(\frac{1}{\rho_v} - \frac{1}{\rho_l} \right) \dot{m}'' \delta(\mathbf{x}_k) d\Gamma \tag{3}$$

where \mathbf{v} is the velocity, ρ is the specific mass, δ denotes the Dirac Delta function, and \mathbf{x}_k is the position of the interface Γ . Considering low Mach number flows with low temperature variations, divergence-free conditions can be expected (except at the interface when phase changes occur).

The momentum balance equation is given by [3]

$$\rho \left(\frac{\partial \mathbf{v}}{\partial t} + \nabla \cdot (\mathbf{v}\mathbf{v}) \right) = -\nabla p + \nabla \cdot [\mu(\nabla \mathbf{v} + (\nabla \mathbf{v})^T)] + \rho \mathbf{g} + \mathbf{f}_{st} + \mathbf{f}_{recoil} \tag{4}$$

where p is the pressure, μ is the dynamic viscosity, \mathbf{g} is the acceleration due to gravity, \mathbf{f}_{st} is a source term to take into account the effects of surface tension, and \mathbf{f}_{recoil} is a source term which computes the effects of the recoil force at the interface.

The effects of surface tension are included in the formulation using the model of Brackbill et al. [16]. This model specifies the surface tension force per unit volume as

$$\mathbf{f}_{st} = \frac{\rho \sigma \kappa \nabla \alpha}{\frac{1}{2}(\rho_l - \rho_v)} \tag{5}$$

where σ is the surface tension coefficient, κ is the local curvature, and α is the volume fraction of the dispersed phase.

Since this study deals with isobaric phenomena, which only involved weak pressure gradients due to dynamical effects, the energy equation was formulated using the internal energy as a primitive variable, as recommended by Tanguy et al. [6]. The energy equation also has a source term using a Dirac Delta function to model the energy transferred at the interface due to phase change [6]:

$$\rho Cp \frac{DT}{Dt} = k \nabla^2 T - \int_{\Gamma} \dot{m}'' L \delta(\mathbf{x}_k) d\Gamma \tag{6}$$

where Cp is the fluid thermal capacity. The additional term in the energy equation corresponds to the amount of energy employed in a phase change whenever a corresponding mass source term was also added. The source term in the energy equation is important in order to assure the correct calculations of the thermal fluxes at the interface [2] which is used to compute the mass density flux.

2.2 Additional term in the non-divergent form of the momentum equation

The mass balance at the bulk of each phase is given by [15]

$$\frac{\partial(\alpha\rho)}{\partial t} + \nabla \cdot (\alpha\rho\mathbf{v}) = 0, \quad (7)$$

where α represents the volume fraction from the continuous phase. Since the flow is incompressible, the mass conservation at each phase is given by [15]

$$\nabla \cdot \mathbf{v} = 0. \quad (8)$$

On the other hand, considering a fluid particle placed at the interface, an additional source term emerges due to the phase change, in order to take into account the variations of the specific mass in these cells during an expansion or contraction of the volume. Assuming an incompressible flow, the mass balance includes a source term at the interface cells, given by the following expression:

$$\nabla \cdot \mathbf{v} = \int_{\Gamma} \left(\frac{1}{\rho_v} - \frac{1}{\rho_l} \right) \dot{m}'' \delta(\mathbf{x}_k) d\Gamma. \quad (9)$$

An interesting remark about the momentum equation in phase change problems which has not yet been noted in the literature is the appearance of an additional force term in the non-divergent form compared to the divergent form. An additional force term appears due to the nonzero velocity divergence in the continuity equation at the interface cells. Until the present moment, the literature has not pointed out the difference between the divergent and non-divergent forms of the momentum equation. This difference will be described and quantified later in the numerical results section.

Transforming the momentum equation to the non-divergent form from the divergent form, the expression of the continuity equation appears naturally due to the product rule for derivatives, as shown in the following expression:

$$\begin{aligned} \frac{\partial(\rho\mathbf{v})}{\partial t} + \mathbf{v} \cdot (\rho\mathbf{v}) &= \rho \left[\frac{\partial\mathbf{v}}{\partial t} + (\mathbf{v} \cdot \nabla)\mathbf{v} \right] + \underbrace{\mathbf{v} \left[\frac{\partial\rho}{\partial t} + \nabla \cdot (\rho\mathbf{v}) \right]}_{\text{extra - term}} \\ &= \rho\mathbf{g} + \nabla \cdot \bar{\sigma} + \mathbf{f}_\sigma. \end{aligned} \quad (10)$$

Since the continuity equation is nonzero over the interface cells, an additional term appears at the interface cells due to the phase change. This additional force is modeled by the mass balance source term which is defined in the following expression only at the interface:

$$\rho \left[\frac{\partial\mathbf{v}}{\partial t} + (\mathbf{v} \cdot \nabla)\mathbf{v} \right] + \underbrace{\mathbf{v} \left[\int_{\Gamma} \rho \left(\frac{1}{\rho_v} - \frac{1}{\rho_l} \right) \dot{m}'' \delta(\mathbf{x}_k) d\Gamma \right]}_{\text{extra - term}} = \rho\mathbf{g} + \nabla \cdot \bar{\sigma} + \mathbf{f}_\sigma. \quad (11)$$

Therefore, the non-divergent form naturally imposes an additional force due to the phase change which is not explicitly present in the divergent form of the momentum equation. The simulations treated in the present paper were performed in the non-divergent form, and tests were conducted to compare the effects of this additional force in the non-divergent form of the momentum equation.

3 The numerical method

This section presents the numerical details of the presented research, which was developed using the homemade code MFSim.

3.1 Phase change model

The phase change model employs an approach similar to Tanguy et al. [6] in order to account for an adequate mass, momentum, and energy transport across the interface. The phase change amount is predicted using the thermal transfer information at the interface and considering the energy source term as the latent energy relevant to the phase change in the interface cells when solving the energy equation [21].

In order to compute the temperature gradients at the interface to estimate the mass density flux, the interface is assumed to be at saturation temperature and the volume of fluid (VOF) method is used to construct the proper thermal flux, as previously described by Welch and Wilson [2]. The interface temperature was assumed to be constant in time, which is a common simplification appropriate for most cases with low effects of thermal resistance and pressure jump, as previously investigated by Juric and Tryggvason [3]. Much of the phase change literature has employed this simplification, which is adequate for modeling classical and even complex problems, cf. Tanguy et al. [6] and Pan et al. [7]. Therefore, the interface temperature variations in time have been ignored.

A VOF method [22] was applied to determine the position of the interface and the transport. VOF employs a color function $\varphi(\mathbf{x}, t)$ to indicate the fractional amount of fluid present at a certain position \mathbf{x} and time t . The color function φ was calculated using the following equation [23]:

$$\frac{\partial\varphi}{\partial t} + [\mathbf{v}_{\text{normal}} \cdot \nabla\varphi] = 0. \quad (12)$$

If no phase change occurs, the interface velocity is equal to the fluid velocity at the interface. Otherwise, the interface velocity should be computed with the fluid motion and using a phase change component [6, 15], as shown in the following expression:

$$\mathbf{v}_{\text{normal}} = \mathbf{v}_{\text{fluid - motion}} + \mathbf{v}_{\text{phase - change}}. \quad (13)$$

The velocity component due to a phase change is defined according to the mass density flux previously calculated [15].

$$\mathbf{v}_{\text{phase-change}} = \dot{m}'' \left(\frac{1}{\rho_v} - \frac{1}{\rho_l} \right) \mathbf{n} \quad (14)$$

The imposition of a constant mass density flux allows an exact solution for the interface velocity when the fluid motion does not affect the interface position. Therefore, expression 13 is useful for the purpose of validating static problems, as previously described by Tanguy et al. [6] and Lee et al. [15].

3.2 Interface treatment for pressure

The whole domain formulation treats the interface as diffuse, using the Delta function method (Delta). The earliest work on phase change used the Delta method, described in Welch [2] and Juric and Tryggvason [3]. In this approach, the jump conditions at the interface are expressed by introducing singular source terms in the equations.

In the Delta method, an additional source term is placed for the temporal discretization of the momentum equation according to the following algorithm [6]:

$$\mathbf{v}^* = \mathbf{v}^n - \Delta t \left[\mathbf{v}^n \cdot \nabla \mathbf{v}^n - \frac{\nabla \cdot (2\mu D^n)}{\rho^{n+1}} + \frac{\sigma \kappa \mathbf{n}}{\rho^{n+1}} - \mathbf{g} - \mathbf{f}_{\text{recoil}} \right], \quad (15)$$

$$\nabla \cdot \left(\frac{\nabla p^{n+1}}{\rho^{n+1}} \right) = \frac{\nabla \cdot \mathbf{v}^*}{\Delta t} - \frac{\int_{\Gamma} \left(\frac{1}{\rho_v} - \frac{1}{\rho_l} \right) \dot{m}'' \delta(\mathbf{x}_k) d\Gamma}{\Delta t}, \quad (16)$$

$$\mathbf{v}^{n+1} = \mathbf{v}^* - \Delta t \frac{\nabla p^{n+1}}{\rho^{n+1}}, \quad (17)$$

where D is the deformation tensor.

On the other hand, the jump condition formulation treats the interface as sharp by using the GFM, described in Liu et al. [24], who developed a GFM to capture sharp interface boundary conditions in multiphase flows. They proposed a boundary condition capturing approach for the variable coefficient Poisson equation on domains with an embedded interface. In this approach, the equations are written in each phase separately and additional jump conditions have to be imposed at the interface to respect mass conservation. The GFM treats the Poisson equation with both variable coefficients, and a discontinuous solution can be obtained, according to Liu et al. [24]; alternatively, the Delta method uses a projection method to solve the momentum and Poisson equations with a source term.

Finally, in the GFM method, the pressure must respect the following jump condition [6]:

$$[p]_{\Gamma} = \sigma \kappa - \left(\frac{1}{\rho_v} - \frac{1}{\rho_l} \right) \dot{m}''^2, \quad (18)$$

where the second term represents the recoil pressure occurring with a phase change [6]. This term represents the pressure jump condition due to a recoil force presence at the interface. A vapor recoil force appears due to the fluid's expansion while transforming liquid to vapor [4].

3.3 Computational details

A two-step projection method [25] was used with an explicit treatment of advection terms and with an implicit treatment for pressure and for diffusion terms. The Barton scheme [26] was used for the spatial discretization of the advective terms. The Navier–Stokes and energy equations were solved using a multigrid-multilevel solver. The transient equations were solved using a finite volume methodology.

The present paper employed MFSim code to run all the numerical simulations. MFSim code has been developed in the last ten years in cooperation with a large research group and Petrobras scientific support. The MFSim code uses a block-structured composite grid, defined as a hierarchical sequence of nested, progressively finer grid levels. Each level is formed by a set of non-overlapping parallelepipedal grid blocks aligned with the Cartesian coordinate axes; the refinement ratio between two successive levels is two. Convergence criteria for continuity, momentum and energy equations were set to achieve residuals up to 10^{-6} . All simulations were performed in parallel in the Fluid Mechanics Laboratory cluster at the Federal University of Uberlândia, Brazil.

4 Validation of the numerical model

4.1 Numerical validation: boiling simulations with a constant mass density flux

Simulations of bubble growth by phase change were performed imposing a constant and uniform mass flux across the interface. The initial bubble radius was equal to 0.01 m and a spatially uniform and temporally constant mass density flux of 0.10 kg/(m² s) was imposed. The bubble grew until its radius was twice the initial radius. Then, the difference between the exact radius and the numerical radius was computed. The results obtained in the present paper were compared to Tanguy et al. [6], and with the exact solution from Eq. 13.

The boiling simulations at constant rate were performed using the following physical properties: $\rho_{\text{liq}} = 1000 \text{ kg/m}^3$,

$\rho_{\text{vap}} = 1 \text{ kg/m}^3$, $\sigma = 0.07 \text{ N/m}$, $\mu_{\text{liq}} = 0.001 \text{ kg/(ms)}$, and $\mu_{\text{vap}} = 1.78 \times 10^{-5} \text{ kg/(ms)}$. Since the mass density flux was assumed constant, the flow was considered isothermal. An outflow boundary condition was imposed on all the domain faces, and the flow was not subjected to gravity. The mesh consisted of a structured uniform three-dimensional Cartesian grid with configurations of $32 \times 32 \times 32$, $64 \times 64 \times 64$, and $128 \times 128 \times 128$ cells.

It can be shown from Eq. 13 that the bubble radius will evolve linearly with time according to the following expression:

$$R_{\text{exa}}(t) = R_0 + \frac{\dot{m}''}{\rho}t, \tag{19}$$

where $R_{\text{exa}}(t)$ represents the exact bubble radius, R_0 is the bubble's initial radius, and t is the time.

Figure 1 shows the evolution in time of the bubble radius using the Delta and GFM methods.

The error was obtained as the difference between the numerical bubble radius (R_{num}) and its exact value (R_{exa}), which is given by the following expression:

$$\varepsilon(\%) = \frac{|R_{\text{num}} - R_{\text{exa}}|}{R_{\text{exa}}} \times 100. \tag{20}$$

The bubble radius error at the simulation's final time is presented in Table 1 using three different mesh configurations for the Delta and GFM methods. The computed bubble radius in the present paper exhibited low deviation compared to the exact solution, which can be easily seen in Table 1. Using the GFM method, Tanguy et al. [6] and the present paper exhibited no significant error compared to the exact solution. On the other hand, only the present paper presents results from the Delta simulations with low deviation compared to the literature, since the error found by Tanguy et al. [6] was higher than 20% for all the meshes tested.

Table 1 Bubble radius error ε (%) for $\dot{m}'' = 0.10 \text{ kg/(m}^2\text{s)}$

	32^3	64^3	128^3
Tanguy et al. [6]—GFM	0.51	0.22	0.11
Present paper—GFM	1.50	0.50	0.05
Tanguy et al. [6]—Delta	22.5	23.7	24.3
Present paper—Delta	1.51	0.52	0.05

The differences between the exact and computed radii using the GFM, and Delta methods were lower than 2.0% for all the simulations in the present paper. In addition, the error from the Delta simulations was very similar to the error obtained from the GFM simulations for all mesh configurations. Therefore, according to the behavior of the interface evolution in time, both approaches of jump conditions demonstrated accurate results compared to the expected solution.

4.2 Numerical validation: boiling simulations with a variable mass density flux

Numerical simulations of a vapor bubble growth in a superheated liquid domain were conducted using the Delta and GFM methods to take into account the interface jump condition of pressure. The phase change simulations were performed using a Jakob number of 2.0. The Jakob number (Ja) is defined according to the following equation [6]:

$$Ja = \frac{\rho_{\text{liq}} C_{p\text{liq}}(T_{\infty} - T_{\text{sat}})}{\rho_{\text{vap}} L}. \tag{21}$$

The following physical properties were adopted in the phase change simulations with a variable mass density flux: $\rho_l = 100 \text{ kg/m}^3$, $\rho_v = 1 \text{ kg/m}^3$, $\sigma = 0.01 \text{ N/m}$, $\mu_l = 0.00062 \text{ kg/(ms)}$, $\mu_v = 0.000012 \text{ kg/(ms)}$, $k_l = 0.10 \text{ W/(mK)}$, $k_v = 0.01 \text{ W/(mK)}$, $C_{p\text{liq}} = 20 \text{ J/(kg K)}$, $C_{p\text{vap}} = 10 \text{ J/(kg K)}$, and a latent energy of 1000 J/kg . An outflow boundary

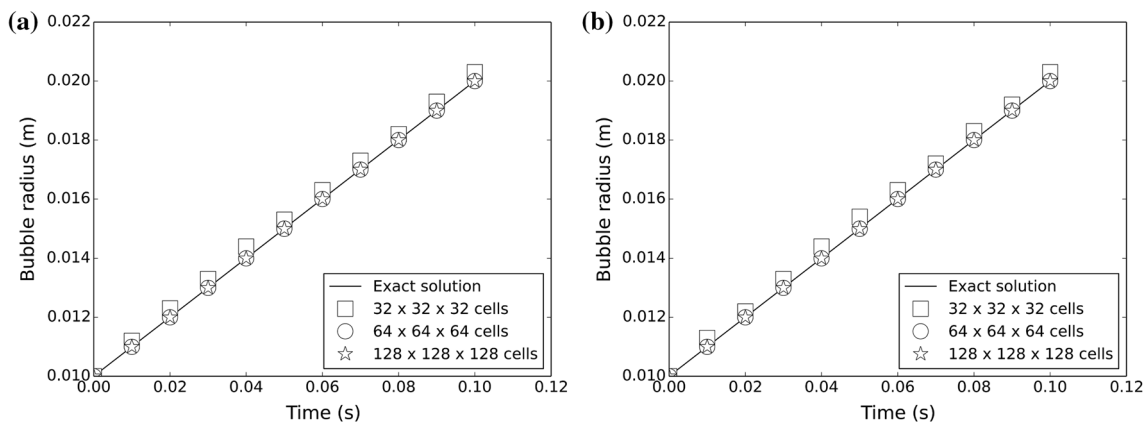


Fig. 1 Bubble radius evolution for $\dot{m}'' = 0.10 \text{ kg/(m}^2\text{ s)}$ using the Delta (a) and GFM (b) methods

condition was imposed on all domain faces, and the flow was not subjected to gravity. AMR simulations were performed with three or four mesh levels and the base level presented the configuration of $16 \times 16 \times 16$ cells.

The numerical model validation was conducted according to the error of the bubble radius in comparison with an analytical solution available in Scriven [27]. The analytical solution describes the evolution of the bubble radius in time according to the following expression [27]:

$$r(t) = 2\beta\sqrt{at}. \quad (22)$$

The parameter β is found by solving a transcendental equation in [27], which is derived from the energy and continuity equations in spherical coordinates [6]. Simplified equations were proposed and presented in Scriven [27] and the following expression was adopted to calculate β [27]:

$$\beta = \sqrt{\frac{3}{\pi}} \left\{ \frac{\Delta T}{\left(\frac{\rho_g}{\rho_l}\right) \left[\frac{L}{C_{p_l}} + \left(\frac{C_{p_l} - C_{p_g}}{C_{p_l}}\right) \Delta T \right]} \right\}. \quad (23)$$

The initial radius of the bubble was 0.0287 m, and the temperature difference between the saturation condition and the superheated liquid was 1.0 K.

Figure 2 shows the evolution of the bubble radius in time in comparison with the analytical solution from Scriven [27]. The grid configuration with three mesh levels was sufficiently fine to provide accurate results, similarly to the mesh with four levels. Good agreement was obtained between the computed bubble radius and the bubble radius from the analytical solution.

According to Fig. 2, the simulations using the Delta and the GFM methods for pressure only deviated slightly from the analytical solution. The evolution of the bubble radius was close to the expected solution provided by Scriven [27] from the beginning until the end of the simulation time.

Figure 3 presents the mesh configuration for the Delta method at the 0 s and at 3.6 s.

The spurious currents from the simulations in Fig. 3 presented approximately the same order of magnitude as the interface velocity, as previously found by Tanguy et al. [6]. Considering that the mass density flux in the simulation was close to $0.01 \text{ (kg/m}^2 \text{ s)}$, it was expected that the spurious currents from the Delta and the GFM methods would be similar, since Section 4.4 shows that the Delta method produced spurious currents with magnitude similar to GFM for $m'' < 1.0 \text{ (kg/m}^2 \text{ s)}$.

5 Results and discussion

5.1 Analysis of the recoil force in momentum equation

According to Nikolayev et al. [4], the importance of the recoil force increases in the vicinity of the critical point of a substance since the magnitude of the surface tension force becomes closer to the magnitude of the recoil force. Therefore, numerical simulations of bubble growth by phase change were performed near the critical point. Numerical simulations of water vapor condensation near critical pressure were performed using the fluid properties presented in Table 2.

This simulation was previously conducted by Lee et al. [15] using the recoil force term in the mathematical model. The diffuse interface treatment was applied to the pressure in the phase change simulations. In addition, the latent energy was 276.4 kJ/kg , the surface tension coefficient was $7.0 \times 10^{-5} \text{ N/m}$, and the temperature difference between the vapor and the liquid was 1 K. Numerical simulations using AMR were conducted with three mesh levels, and the base level presented the configuration of $24 \times 24 \times 24$ cells. The interface presence was considered the refinement criterion.

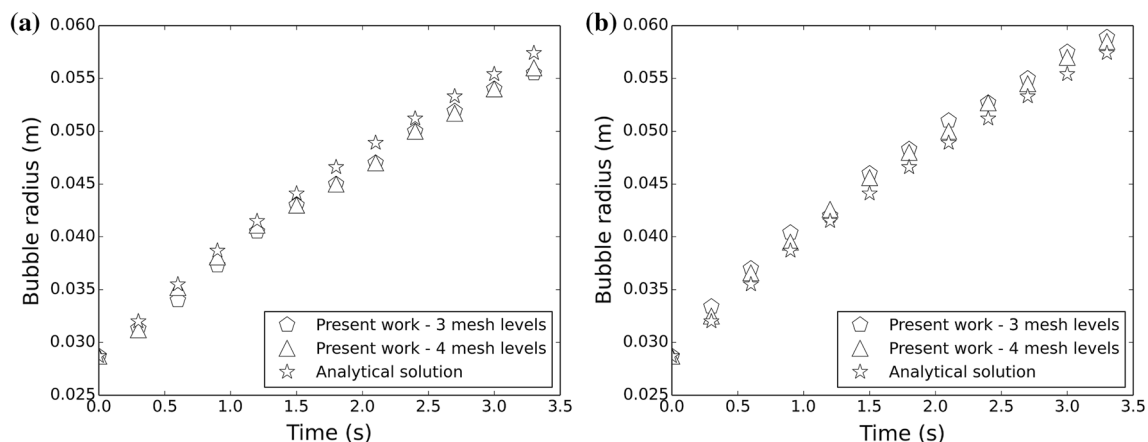


Fig. 2 Bubble radius evolution using **a** the Delta method and **b** the GFM method

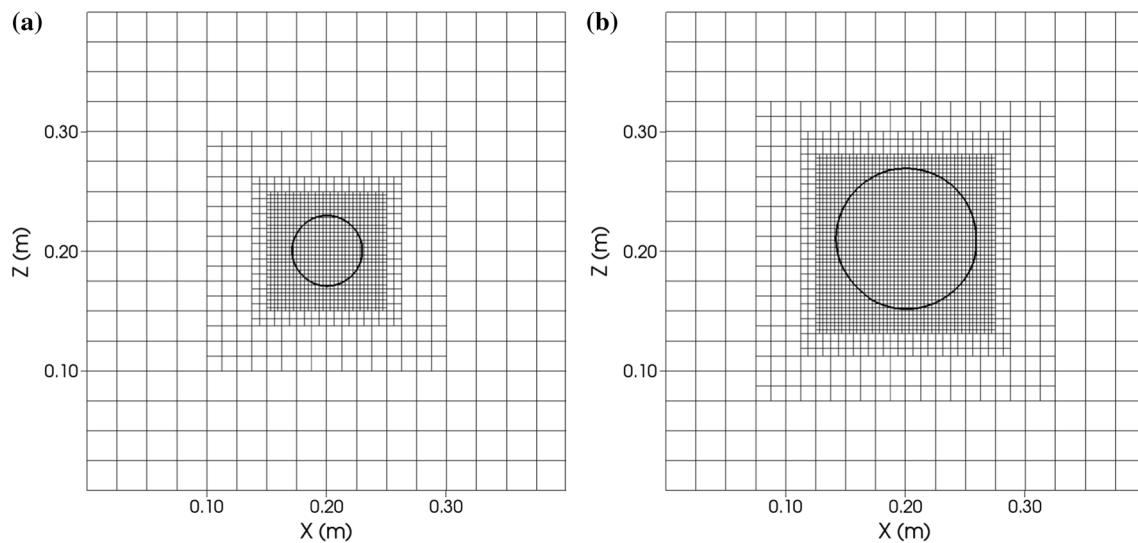


Fig. 3 Slice of the central xz -plane showing the interface and mesh configuration using the Delta method considering a variable mass density flux with $Ja = 2.0$

Table 2 Fluid properties of saturated water at near critical pressure

Phase	ρ (kg/m ³)	μ (μ Pa s)	C_p (J/kg K)	k (W/mK)
Vapor	242.7	32.38	3520	0.538
Liquid	402.4	46.7	2128	0.545

As previously seen in the last subsection, the bubble radius evolves linearly with time according to expression 18. Figure 4 presents the bubble radius evolution in time from the simulations, both including and excluding the term that models the effects of the recoil force in the momentum equation.

Figure 4 shows good agreement between the exact solution and the results presented here for the simulation with a constant mass density flux of $0.01 \text{ kg/m}^2 \text{ s}$. As expected, the evolution of the bubble radius was linear in time since the mass density flux was taken to be constant.

Figure 5 shows the magnitude of the surface tension force effects compared to the magnitude of the recoil force term.

According to the data collected during the simulation, the magnitude of the recoil force was approximately five orders of magnitude lower than the surface tension force. Since the inertial and surface forces were bigger than the recoil force in the momentum equation in the case investigated, the addition or not of the recoil force had only insignificant effects on the bubble rate movement. Raghupathi et al. [17] also found only an insignificant influence of the recoil force term in similar simulations of phase change.

Until the present moment, the only numerical investigation found in the literature that revealed a significant influence of the recoil force has been Raghupathi et al. [17] for simulations where two different regions of the interface were subjected to

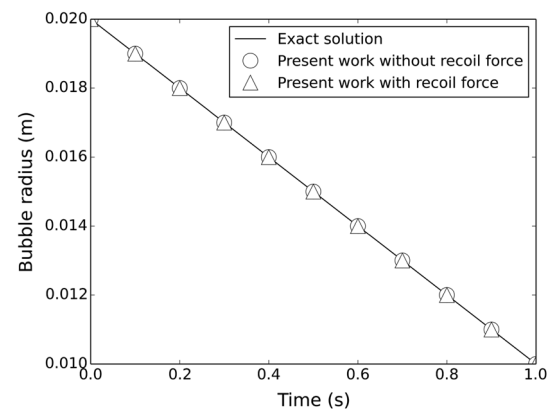


Fig. 4 Bubble radius evolution in phase change simulations with and without the recoil force effects using the Delta method

strong temperature differences, there occurring a visible interface motion due to the recoil force. Therefore, more studies are necessary to understand the influence of the recoil force in phase change problems, especially for engineering applications. In addition, the way the recoil force is being modeled in the literature should be better investigated since alternative approaches could provide a more realistic influence of the recoil force than the expression proposed by Nikolayev [4].

5.2 Analysis of the additional force in momentum equation

In order to quantify the influence of modeling the additional force due to phase change, which appears in the

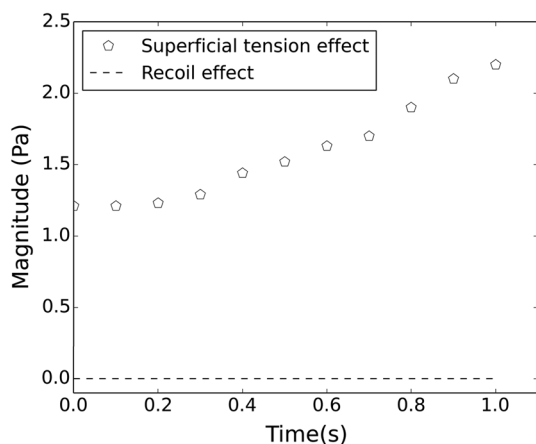


Fig. 5 Magnitude of the effects from the surface tension force compared to the recoil force using the Delta method

non-divergent form of the momentum equation, simulations were performed with and without the extra source term in momentum equation. A constant mass density flux was imposed at the interface, and the effects of this force due to phase change on the time evolution of the interface were evaluated. Simulations of boiling were performed for a intense value of mass density flux and the influence of the extra force term was evaluated.

Simulations of bubble growth by phase change were performed by imposing a constant and uniform mass transfer rate across the interface. This case was previously investigated by Tanguy et al. [6], where the bubble initial radius was equal to 0.01 m and a spatially uniform and temporally constant mass density flux of $0.1 \text{ kg/m}^2 \text{ s}$ was imposed. The bubble grew until its radius was twice the initial radius; then, the difference between the exact radius and the computational radius was computed. The interface evolution was compared to the exact solution provided from Eq. 13.

The simulations were performed using the following physical properties: $\rho_{\text{liq}} = 1000 \text{ kg/m}^3$, $\rho_{\text{vap}} = 1 \text{ kg/m}^3$, $\sigma = 0.07 \text{ N/m}$, $\mu_{\text{liq}} = 0.001 \text{ kg/(ms)}$ and $\mu_{\text{vap}} = 1.78 \times 10^{-5} \text{ kg/(ms)}$. Since the mass density flux was constant, the flow was considered isothermal. The outflow boundary condition was imposed on all the domain faces, and the flow was not subjected to gravity. Numerical simulations using AMR were conducted with three mesh levels, and the base level presented the configuration of $16 \times 16 \times 16$ cells. The interface presence was considered the refinement criterion.

As previously seen in Sect. 4.1, the bubble radius evolves linearly with time according to expression 18. Figure 6 shows the evolution in time of the bubble radius for the non-divergent form of the momentum equation, both with and without the additional source term from Eq. 10.

The interface evolution was not damaged even with a high mass density flux imposed at the interface. Then, according

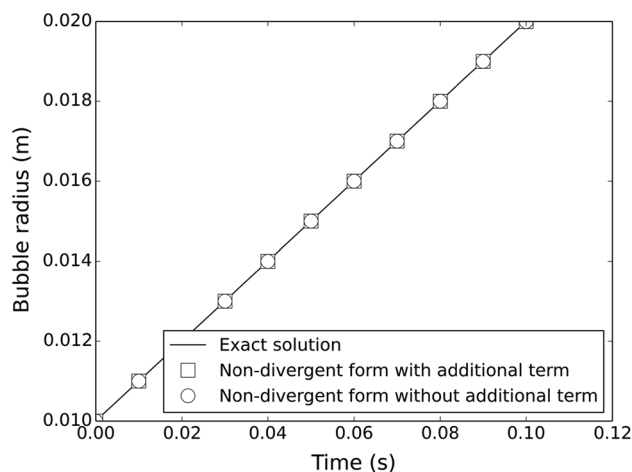


Fig. 6 Bubble radius evolution in the phase change simulations using Delta for the non-divergent form with and without the extra force term from Eq. 10

to the numerical results seen in Fig. 1, the influence of the force due to the phase change at the interface is of little importance for the interface's behavior over time.

The extra force in the momentum equation was about three orders of magnitude lower than the surface tension force effects. The quantification of the additional force demonstrated that its insignificance in the numerical results is a consequence of its magnitudes being smaller than the inertial and interfacial forces. Figure 7 shows the magnitude of the surface tension force effects compared to the magnitude of the additional force term.

The negligible influence of this force term in the non-divergent form of the momentum equation in the simulations performed corroborates previous results in the literature, presenting accurate validation cases while not employing this force term, namely [2, 15] and [6]. Therefore, the influence of this term may be considered of little importance in phase change problems when using the non-divergent form of the momentum equation, although being mathematically inconsistent.

In order to confirm the low influence of this additional term in the mathematical model, simulations using a mass density flux of $10.0 \text{ kg/(m}^2 \text{ s)}$ were performed. The value of this mass density flux is so high that it may be considered even physically impossible. However, the intention is to determine whether this additional term may interfere with the numerical results for extremely high intensities of phase change. The bubble initial radius was 0.1 m and the simulation final time was 0.01 s, when the bubble radius was twice the initial radius.

According to the numerical results obtained, the bubble radius prediction was accurate even for a high mass density flux. The difference between the exact solution and the

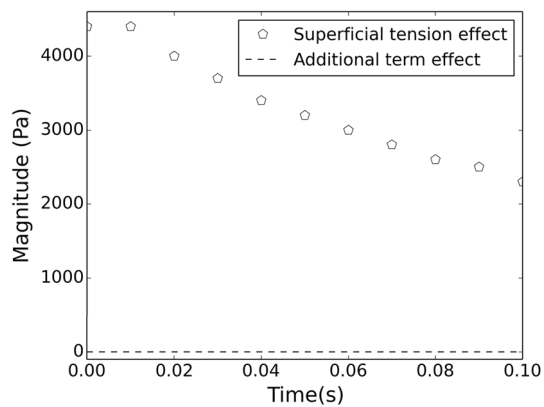


Fig. 7 Magnitude of the effects of the surface tension force compared to the additional force using the Delta method, for $\dot{m}'' = 0.1$

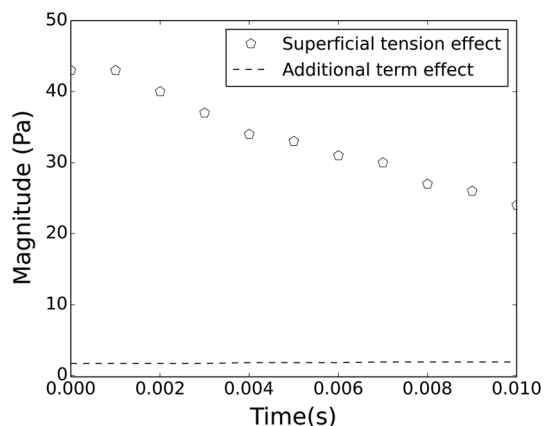


Fig. 8 Magnitude of the effects from the surface tension force compared to the additional force using the Delta method considering $\dot{m}'' = 10.0$

computed bubble radius at the simulation's final time was lower than 1.0%. Figure 8 shows the magnitude of the effects of the surface tension force compared to the magnitude of the additional force term from the simulation considering $\dot{m}'' = 10.0$.

The magnitude of the effects from the additional term is about two orders of magnitude lower than the surface tension force effects. Therefore, as seen in Fig. 8, the additional force term here discussed may be considered irrelevant to phase change problems.

5.3 Analysis of the spurious currents in the simulations of bubble growth

In order to evaluate the spurious currents, phase change simulations were performed with a growing bubble with three different constant and uniform mass density fluxes. The bubble's initial radius was 0.01 m, and the spatially uniform and

temporally constant mass density fluxes of $0.1 \text{ kg}/(\text{m}^2 \text{ s})$, $1.0 \text{ kg}/(\text{m}^2 \text{ s})$ and $10 \text{ kg}/(\text{m}^2 \text{ s})$ were imposed. The mass density flux of $0.1 \text{ kg}/(\text{m}^2 \text{ s})$ (represents a moderate intensity of phase change, which is found in several numerical investigations in the literature, such as Tanguy et al. [6]). This phase change rate is also similar to that found in experimental cases, such as water bubble condensation at atmospheric pressure from Kamei and Hirata [28]. Next, the mass density flux of $1.0 \text{ kg}/(\text{m}^2 \text{ s})$ represents a strong phase change rate, which may refer to an extremely severe thermodynamic condition for phase change. Finally, the mass density flux of $10 \text{ kg}/(\text{m}^2 \text{ s})$ represents an extreme rate of phase change intensity which may be considered even impossible to model on small scales due to the fast speed of the volume change in time. The purpose of evaluating the spurious currents using this high phase change intensity is to draw conclusions about the two methods in the most severe conditions possible.

The time step was set as $1.0 \times 10^{-5} \text{ s}$, and the evaluation of the spurious currents was carried out at 0.001 s. Numerical simulations using AMR were conducted with two mesh levels, and the base level presented the configuration of $32 \times 32 \times 32$ cells. The interface presence was considered the refinement criterion.

Figure 9 shows the velocity fields using the Delta and GFM methods for a mass density flux of $0.1 \text{ kg}/(\text{m}^2 \text{ s})$ at 0.001 s.

The maximum velocity observed in the simulations using the Delta and GFM methods in Fig. 6 was close to 0.0002 m/s. Inside the dispersed phase, both approaches produced some spurious currents, which exhibited similar magnitudes. The mass density flux of $0.1 \text{ kg}/(\text{m}^2 \text{ s})$, in the simulation using Delta, produced a visible velocity field at the interface region, which extended to the domain limits. The simulation using GFM presented a velocity field with low influence of spurious currents outside the bubble. The present paper found spurious currents one order of magnitude lower than Tanguy et al. [6], who obtained spurious currents close to 0.05 m/s using the Delta method and 0.01 m/s using the GFM approach.

Figure 10 shows the velocity fields using the Delta and GFM methods for a mass density flux of $1.0 \text{ kg}/(\text{m}^2 \text{ s})$ at 0.001 s.

The velocity field obtained from the simulation using the GFM method presented smaller spurious currents compared to the Delta method. The simulation using the GFM method has only small velocities inside the dispersed phase; outside the bubble, there are no spurious currents. The magnitude of the spurious currents in the simulation using the Delta method was twice that of the velocities obtained in the GFM method. Figure 11 shows the velocity fields using the Delta and GFM methods for a mass density flux of $10.0 \text{ kg}/(\text{m}^2 \text{ s})$ at 0.001 s.

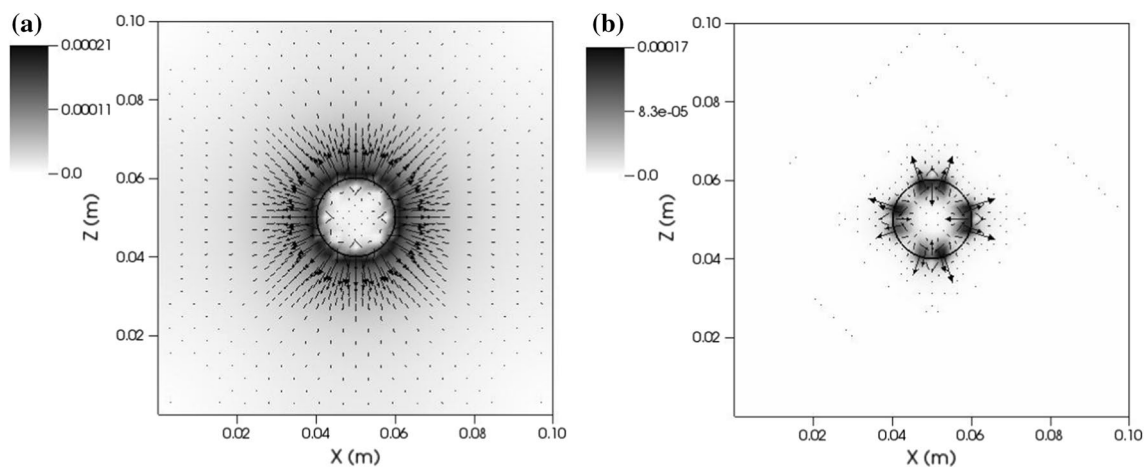


Fig. 9 Spurious currents for $\dot{m}'' = 0.1 \text{ kg}/(\text{m}^2 \text{ s})$ at 0.001 s, **a** with Delta and **b** with GFM

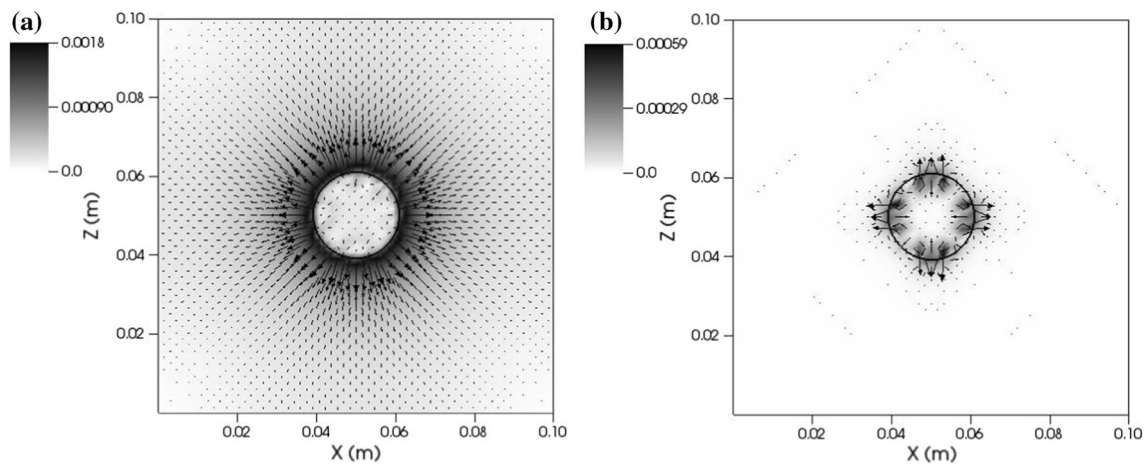


Fig. 10 Spurious currents for $\dot{m}'' = 1.0 \text{ kg}/(\text{m}^2 \text{ s})$ at 0.001 s, **a** with Delta and **b** with GFM

The simulation considering a mass density flux of $10.0 \text{ kg}/(\text{m}^2 \text{ s})$ produced a spurious velocity field with significant magnitudes with the Delta method compared to the GFM method. The maximum velocities were observed in the proximities of the interface and the spurious currents extended to the limits of the domain. The simulation using the GFM method presented smaller spurious currents than the Delta method, and they were two orders of magnitude lower than for Delta.

The numerical results of the magnitudes of the spurious currents in the simulations were expected, since the GFM method treats the interface as sharp by defining ghost cells, preserving a behavior that is more physically consistent with an interface. As described by Tanguy et al. [6], preserving the sharpness of the velocity field allows transporting the interface with an adequate velocity, which is zero in the present case, since the bubble is stationary. Therefore, the

GFM method minimized the numerical diffusion across the interface, which is particularly important in phase change problems.

According to the velocity fields obtained from the simulations using the Delta method, a mass density flux of $0.1 \text{ kg}/(\text{m}^2 \text{ s})$ did not produce noticeable spurious currents compared to the velocity fields from the GFM approach. On the other hand, a mass density flux of $1.0 \text{ kg}/(\text{m}^2 \text{ s})$ or higher did increase excessively the spurious currents in the simulations using the Delta method, in comparison with the GFM approach. Therefore, the magnitude of the mass density flux directly affected the intensity of the spurious currents obtained in the simulations with the Delta method.

Table 3 summarizes the magnitudes of the spurious currents found at the end of the simulation, using the Delta and GFM approaches, with mass density fluxes of $0.1 \text{ kg}/(\text{m}^2 \text{ s})$, $1.0 \text{ kg}/(\text{m}^2 \text{ s})$, and $10.0 \text{ kg}/(\text{m}^2 \text{ s})$.

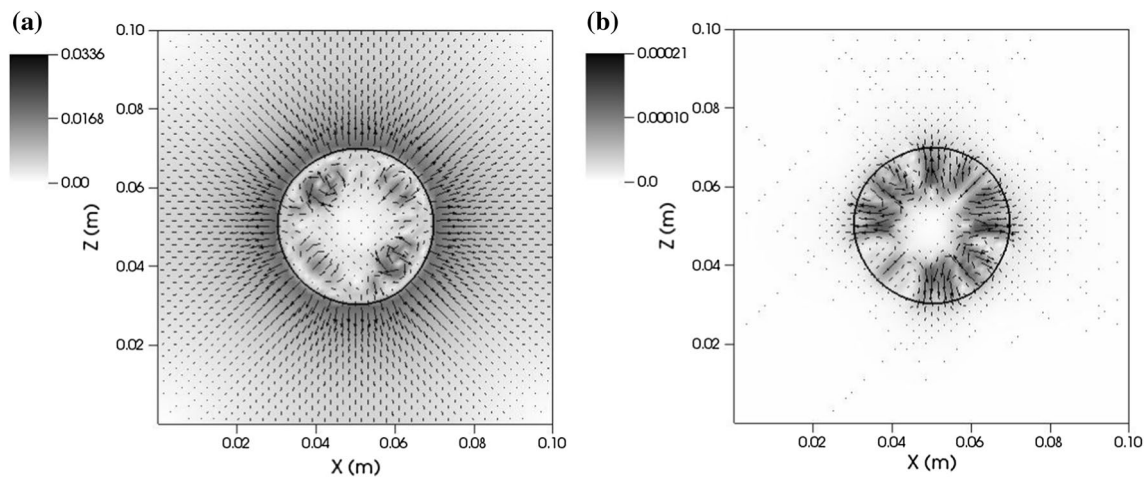


Fig. 11 Spurious currents for $\dot{m}'' = 10.0 \text{ kg}/(\text{m}^2 \text{ s})$ at 0.001 s, **a** with Delta and **b** with GFM

Table 3 Spurious currents using different \dot{m}'' for Delta and GFM methods at 0.001 s

Mass density flux $\text{kg}/(\text{m}^2 \text{ s})$	Delta (m/s)	GFM (m/s)
0.1	0.0002	0.0001
1.0	0.0018	0.0005
10.0	0.0330	0.0002

Table 4 Assessment of mesh configuration in the simulations with $\dot{m}'' = 0.1 \text{ kg}/(\text{m}^2 \text{ s})$

	Time (s)	Number of cells	ϵ (%)	η (%)
Uniform grid	1440	884,736	0.05	–
AMR—two levels	480	157,248	0.06	53.3
AMR—three levels	300	74,304	0.07	40.3
AMR—four levels	240	66,304	0.09	45.0

5.4 Analysis of the grid configuration in simulations of the growth of a bubble

Uniform grid and AMR simulations were evaluated in order to quantify the AMR efficiency compared to the uniform grid simulations, considering a mass density flux of $0.1 \text{ kg}/(\text{m}^2 \text{ s})$. The simulations were performed using the properties and the physical model previously described in Sect. 4.1 with the Delta method of pressure interface treatment. The AMR simulations were performed with two, three, and then four levels of mesh refinement, with the most refined level being $128 \times 128 \times 128$ cells.

In order to present a quantitative analysis of the AMR efficiency, the efficiency was calculated using an expression from Akhtar and Kleis [12] which uses the time and number of cells employed in the simulations. The expression for AMR efficiency (η) is given by the following equation [12]:

$$\eta(\%) = \frac{t_{\text{uni}} n_{\text{ada}}}{t_{\text{ada}} n_{\text{uni}}} \tag{24}$$

where t_{uni} is the simulation time using a uniform grid, n_{uni} is the number of cells in the simulation using a uniform grid, t_{ada} is the simulation time using AMR, and n_{ada} is the number of cells in the simulation using AMR.

Table 4 presents the computational time spent on the simulation, the number of cells employed, the error of the bubble radius prediction (ϵ), and the AMR efficiency (η). It can be seen that the coarse grid regions represent more than half of the domain’s total volume, especially at the beginning of a simulation. In addition, using a coarse grid away from the interface implies a significant reduction of the number of computational cells. Therefore, AMR is a numerical tool which can reduce the computational costs for two-phase flow problems with phase change and allow more efficient simulations.

Two main advantages of using AMR instead of uniform grids were the reduction in the number of cells employed and the computational time needed. According to the results shown in Table 4, the uniform grid employed almost 900,000 cells, while AMR used close to 160,000 cells with two levels and almost 75,000 cells with three levels. Therefore, the use of AMR reduced the number of cells by more than 10 times compared to uniform grid simulations. Moreover, the computational time needed to finish the simulation was almost five times lower using an adaptive mesh with three levels compared to a uniform grid. Lastly, it can be seen that the errors of the uniform grid and AMR simulations are similar, since the error of the bubble radius was always below 1%. Therefore, according to Table 4, AMR yielded accurate

results with lower computational costs compared to uniform grids and revealed a great potential to be adopted in phase change simulations.

Concerning the AMR efficiency, the present efficiencies analyzed in this paper were approximately 50%. On the other hand, Akhtar and Kleis [12] found an efficiency close to 70% for similar simulations of boiling. Probably the AMR efficiency in the research presented here is lower than Akhtar and Kleis [12] since the latter used octree grids, which uses a simplified algorithm, reducing the time required to solve all the equations in each computational cell.

6 Case study: simulation of film boiling with Rayleigh–Taylor instability

Pool boiling systems are widely encountered on the ground and in outer space applications [29]. Film boiling is an important phase change phenomenon since it is present in several applications in the engineering field [30]. In addition, film boiling is one of more ideal pool boiling regimes to validate a method, due to its lesser complexity [15]. A particular case of film boiling is the development of Rayleigh–Taylor instability, which is widely reported in the phase change literature.

Rayleigh–Taylor instability is the result of a baroclinic torque created by the misalignment of the pressure and specific mass gradients at an interface [31]. Rayleigh–Taylor instability occurs when a heavy fluid initially lies above a lighter one in a gravitational field [30], promoting a baroclinic torque. The baroclinic torque is mathematically represented in the transport equation of vorticity (ω), which can be obtained by taking the curl of the momentum equation, and is given by the following equation:

$$\frac{D\omega}{Dt} = -(\omega \cdot \nabla)\mathbf{v} + \frac{(\nabla\rho \times \nabla p)}{\rho^2} + (\omega \cdot \nabla)\mathbf{v} + \frac{1}{Re}(\nabla^2\omega) \quad (25)$$

The baroclinic contribution is represented by the term $\frac{(\nabla\rho \times \nabla p)}{\rho^2}$ and is always perpendicular to the specific mass gradient. If the specific mass and pressure gradients are aligned, this term is zero.

This instability has a particularly important application in inertial confinement fusion [32]. Although Rayleigh–Taylor instability is rarely observed in its authentic form, it plays an important role in various natural and technological processes. The formation of bubbles from a vapor film beneath a liquid in film boiling is a classic example of a relatively authentic Rayleigh–Taylor instability [33]. Sharp [30] enumerated some examples of Rayleigh–Taylor instabilities in nature and in technological fields, such as the overturn of the outer portion of the collapsed core of a massive star, the formation of high-luminosity twin-exhaust jets in rotating gas clouds in

an external gravitational potential, laser implosion of deuterium–tritium fusion targets, electromagnetic implosion of a metal liner and several others.

The present paper will also investigate numerical simulations of film boiling using the diffuse interface treatment for pressure. The simulations were performed using AMR and uniform grids. The thermal transfer rate will be compared to an experimental correlation from Berenson [34], which predicts the thermal transfer rate at a heated wall where pool boiling occurs. Berenson's [34] experimental correlation defines the mean Nusselt number at the heated wall according to the following expression:

$$Nu = 0.425 \left(\frac{GrPr}{Ja} \right)^{1/4}, \quad (26)$$

where the Prandtl number is 1.0, the Jakob number is 1.0, and the Grashof number is 304.3.

The thermo-physical properties of the fluid used in the simulations has the same ratio between the liquid and vapor phase as that in Akhtar and Kleis [12], as given in Table 5.

In the simulation of film boiling, a vapor film completely covers the heated surface. During the entire simulation, the denser liquid above the vapor film falls, due to the action of gravity, and at the same time the interface between the liquid and vapor rises away from the heated wall. As the liquid moves closer to the heated wall, evaporation at the liquid–vapor interface prevents the liquid from getting into contact with the wall. Since the intensity of the baroclinic torque increases with time, an interface peak at the center of the domain emerges.

The physical model in the simulations consists of a three-dimensional domain subjected to gravity. The lateral boundaries are symmetric, and an outflow boundary condition is used at the top surface. Moreover, a constant temperature is imposed at the bottom wall:

$$T_{\text{wall}} = T_{\text{sat}} + \Delta T. \quad (27)$$

The bottom wall was kept at a fixed temperature, higher than the temperature of the top and lateral walls, similarly to the procedure adopted by Akhtar and Kleis [12]. The computational domain was subjected to a grid independence study, and a validation was performed using the mean Nusselt number at the bottom wall. Figure 12 illustrates a slice from the central xz -plane with the interface position for three grid configurations: $32 \times 32 \times 64$, $64 \times 64 \times 128$ and $128 \times 128 \times 256$ cells.

Figure 12 shows that the two highest mesh resolutions closely match each other (dashed and dotted lines). On the other hand, the coarsest grid presented a very different profile from the other grid configurations, due to the insufficient

Table 5 Assessment of mesh configuration in the simulations of film boiling

ρ_l/ρ_v	μ_l/μ_v	k_l/k_v	Cp_l/Cp_v
4.78	2.59	3.56	0.66

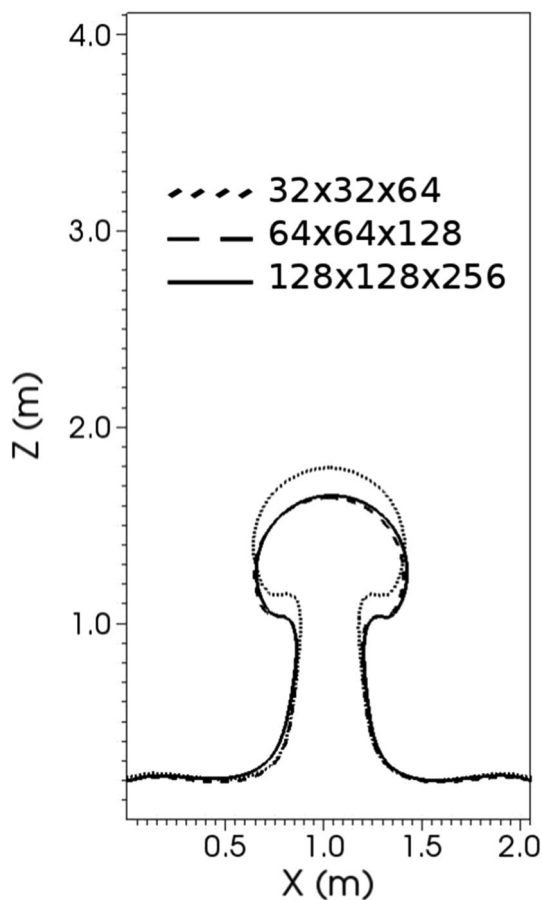


Fig. 12 Interface at time 12.0 s where the dotted line represents the mesh of $32 \times 32 \times 64$ cells, the dashed line is the mesh configuration of $64 \times 64 \times 128$ cells, and the continuous line shows the grid with $128 \times 128 \times 256$ cells

mesh quality. Therefore, the mesh with the configuration of $64 \times 64 \times 128$ cells was considered adequate to model film boiling.

In order to validate the Nusselt number at the bottom wall using an experimental correlation from the literature, a simulation using a uniform grid was performed using the configuration of $64 \times 64 \times 128$ cells and an AMR simulation was performed with three mesh levels. The most refined level in the AMR simulation presented the same mesh width as the uniform grid simulation.

Figure 13 shows two moments in the simulation of film boiling, namely the beginning and the end of the simulation time.

The two coherent structures composing the Rayleigh–Taylor instability are evident in Fig. 13 at the final time of the simulation. There are four noticeable spikes (fluid structure of heavy fluid growing into light fluid) and one mushroom-shaped bubble (fluid structure of light fluid growing into heavy fluid). As Fig. 13 shows, the stem does not pinch off.

Figure 14 shows the interface contour and the grid configuration employed at the initial time of the simulation and at the final time.

Adaptive mesh refinement promoted a great reduction of the computational costs. As Fig. 14 shows, the regions away from the interface used a coarse grid, which helped the simulation to run faster than with a uniform grid. Since the interface was the region where the phenomenon was developed, the other regions of the domain were solved with a relatively coarse grid.

Table 6 shows the time necessary to run the simulation using AMR and uniform grids, as well as the mean number of cells used in each simulation.

Fig. 13 Interface **a** at the initial time of the simulation and **b** at the final time

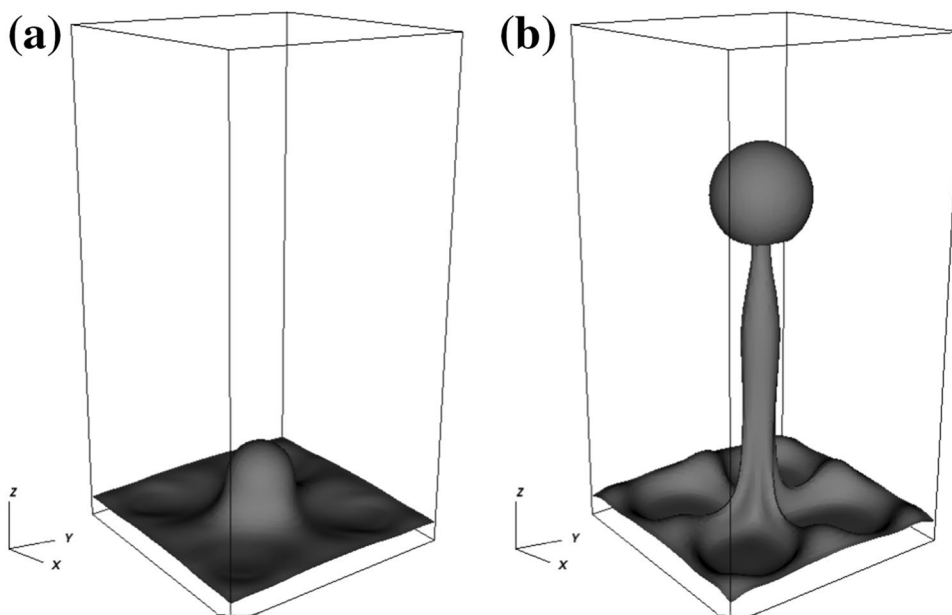


Fig. 14 Interface and mesh configuration **a** at the initial time of the simulation and **b** at the final time

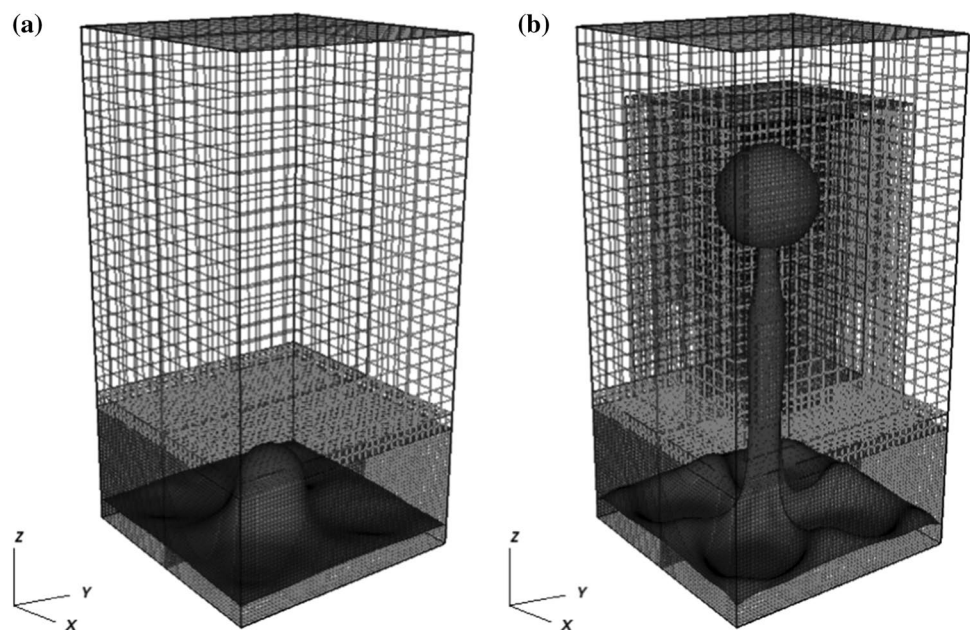


Table 6 Assessment of mesh configuration in the simulations of film boiling

	Time (s)	Number of cells	Mean Nusselt number difference (%)
AMR	57,600	172,000	2.5
Uniform grid	82,800	524,288	2.3

According to Table 6, AMR promoted a reduction of approximately 30% of CPU time compared to the simulation using uniform grids. As expected, the number of cells employed in the AMR simulation was significantly lower than the uniform grid simulation. The reduction of nearly 67% from the total number of cells sharply reduced the computational power required. Thus, AMR simulations have again achieved accurate results while saving computational power and the time necessary to run the simulations.

According to expression 21, the AMR efficiency was approximately 47%, representing a great improvement of efficiency. Akhtar and Kleis [12] evaluated the AMR efficiency using that expression and found approximately 52% at a simulation time of 1.0 s, which corroborates the efficiency obtained in the present paper.

The experimental correlation of Berenson [34] will now be used for the minimum thermal flux, which is the condition where there is a stable vapor film over the heating surface. The mean Nusselt number can be computed at the bottom wall and is presented in Fig. 15 in comparison with the solution from Berenson [34].

As previously seen in Akhtar and Kleis [12], the mean Nusselt number remains approximately constant after some

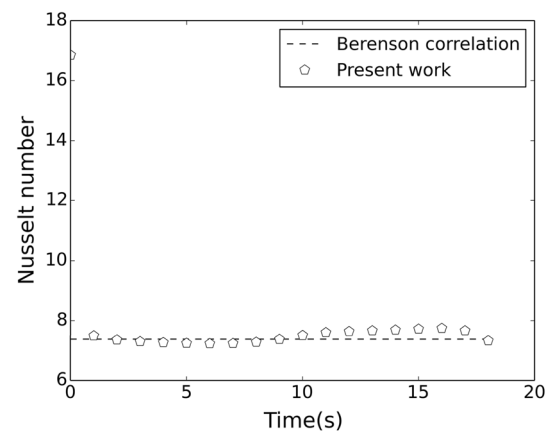


Fig. 15 Evolution in time of the mean Nusselt number in the film boiling simulation

time, according to Fig. 15. A good agreement was found between the computational results obtained in the present work and the experimental correlation from Berenson [34]. Therefore, the computational results in this subsection confirmed the accuracy of the model for complex phase change problems using a diffuse interface treatment with accuracy and physical consistency.

According to the results from the simulations of film boiling with the development of Rayleigh–Taylor instability, the diffuse interface treatment for pressure demonstrated good accuracy, which was confirmed by the validation of the local thermal transfer rate and the physical behavior expected from the theory of stability analysis according to the visualization of the baroclinic torque action in the simulations.

7 Conclusions

The present paper has pointed to a difference between modeling phase change problems using the divergent form of the momentum equation and its non-divergent form. This difference was subjected to a quantitative analysis to evaluate the importance of the additional force term in the non-divergent form of the momentum equation. The numerical results showed no significant effects.

The influence of the recoil force was not noticeable in the evolution of the interface of a condensation bubble, even near the critical point. The quantification of the recoil force demonstrated that the surface tension forces dominate in importance the recoil term in the momentum equation. More studies in different applications are needed to determine whether modeling this force is relevant for phase change problems.

Phase change simulations with a constant mass density flux provided information about the occurrence of spurious currents and interface evolution in time using sharp and diffuse interface treatments for pressure. Phase change simulations using the Delta approach presented adequate numerical results, in accordance with the literature; however, the presence of spurious currents was observed in cases of high mass density fluxes. On the other hand, the simulations using the GFM method presented smaller spurious currents than the Delta method, even with a high mass density flux. The bubble radius prediction demonstrated no relevant differences between either approach and the exact solution, for any of the simulations performed. The authors of the present paper conclude that the Delta method has potential as an interface treatment suitable for pressure for most parts of phase change rates, since the presence of spurious currents did not negatively influence the interface evolution.

Concerning the phase change simulations with a variable mass density flux, the bubble radius prediction presented good agreement with an analytical solution for the bubble radius in the literature. The spurious currents had magnitudes close to the calculated interface velocity from the mass density flux, as previously seen in the literature for the Delta and GFM methods. Moreover, the numerical model presented results with grid independence and showed convergence to the reference validation results.

The AMR simulations promoted time saving by limiting the need for a fine uniform grid over the whole domain. Large computational costs were spared using AMR, because of the considerable reduction in the number of computational cells required. Moreover, accurate numerical results were obtained using AMR. Thus, AMR is suggested as an important numerical strategy to perform phase change simulations. The AMR efficiency was computed in several cases, and similar results were obtained to those in the literature.

In addition, the refinement criterion of interface presence was considered adequate to perform all the phase change simulations, providing results with good resolution and smaller computational costs compared to the simulations using uniform grids.

Lastly, simulations of film boiling exhibited the robustness of the diffuse interface treatment for pressure in complex problems with multiple interface discontinuities and challenging numerical conditions during the phase change.

Acknowledgements The authors gratefully acknowledge financial support from Petrobras, CNPQ, Fapemig and Capes. The authors are also grateful to the mechanical engineering graduate program from the Federal University of Uberlândia (UFU).

References

- Haelssig J, Thibault A, Etemad S (2010) Direct numerical simulation of interphase heat and mass transfer in multicomponent vapour-liquid flows. *Int J Heat Mass Transf* 53:3947. <https://doi.org/10.1016/j.ijheatmasstransfer.2010.05.013>
- Welch SWJ, Wilson J (2000) A volume of fluid based method for fluid flows with phase change. *J Comput Phys* 160:662. <https://doi.org/10.1006/jcph.2000.6481>
- Juric D, Tryggvason G (1998) Computations of boiling flows. *Int J Multiphase Flow* 24:387. [https://doi.org/10.1016/S0301-9322\(97\)00050-5](https://doi.org/10.1016/S0301-9322(97)00050-5)
- Nikolayev V, Chatain D, Garrabos Y, Beysens D (2016) Experimental evidence of the vapor recoil mechanism in the boiling crisis. *Phys Rev Lett* 97:253. <https://doi.org/10.1103/PhysRevLett.97.184503>
- Strotos G, Gavaises M, theodorakakos A, Bergeles G (2011) Numerical investigation of the evaporation of two-component droplets. *Fuel* 90:1492. <https://doi.org/10.1016/j.fuel.2011.01.017>
- Tanguy S, Sagan M, Lalanne B, Couderc F, Colin C (2014) Benchmarks and numerical methods for the simulation of boiling flows. *J Comput Phys* 264:1. <https://doi.org/10.1016/j.jcp.2014.01.014>
- Pan Z, Weibel J, Garimella SV (2016) A Saturated-Interface-Volume Phase Change Model for Simulating Flow Boiling. *Int J Heat Mass Transf* 93:945. <https://doi.org/10.1016/j.ijheatmasstransfer.2015.10.044>
- Tryggvason G, Lu J (2015) Direct numerical simulations of flows with phase change. *Procedia IUTAM* 15:2. <https://doi.org/10.1016/j.piutam.2015.04.002>
- Tsui Y, Lin SW, Lai YN, Wu FC (2014) Phase change calculations for film boiling flows. *Int J Heat Mass Transf* 70:745. <https://doi.org/10.1016/j.ijheatmasstransfer.2013.11.061>
- Tanguy S, Menard T, Berlemont A (2007) A level set method for vaporizing two-phase flows. *J Comput Phys* 221:837
- Harvie D, Davidson M, Rudman M (2006) An analysis of parasitic current generation in volume of fluid simulations. *Appl Math Model* 30:1056. <https://doi.org/10.1016/j.apm.2005.08.015>
- Akhtar M, Kleis S (2013) Boiling flow simulations on adaptive octree grids. *Int J Multiphase Flow* 53:88. <https://doi.org/10.1016/j.ijmultiphaseflow.2013.01.008>
- Francois MM, Cummins SJ, Dendy ED, Kothe DB, Sicilian JM, Williams MW (2006) A balanced-force algorithm for continuous and sharp interfacial surface tension models within a volume tracking framework. *J Comput Phys* 213:141. <https://doi.org/10.1016/j.jcp.2005.08.004>

14. Samkhaniani N, Ansari MR (2016) Numerical simulation of bubble condensation using CF-VOF. *Progres Nucl Energy* 89:120. <https://doi.org/10.1016/j.pnucene.2016.02.004>
 15. Lee MS, Riaz A, Aute V (2017) Direct numerical simulation of incompressible multiphase flow with phase change. *J Comput Phys* 344:381. <https://doi.org/10.1016/j.jcp.2017.04.073>
 16. Brackbill JU, Kothe DB, Zemach C (1992) A continuum method for modeling surface-tension. *J Comput Phys* 100:335. [https://doi.org/10.1016/0021-9991\(92\)90240-Y](https://doi.org/10.1016/0021-9991(92)90240-Y)
 17. Raghupathi PA, Kandlikar SG (2016) Bubble growth and departure trajectory under asymmetric temperature conditions. *Int J Heat Mass Transf* 95:824. <https://doi.org/10.1016/j.ijheatmasstransfer.2015.12.058>
 18. Ningegowda BM, Premachandran B (2014) A coupled level set and volume of fluid method with multi-directional advection algorithms for two-phase flows with and without phase change. *Int J Heat Mass Transf* 79:532
 19. Nikolopoulos N, Theodorakakos A, Bergeles G (2007) A numerical investigation of the evaporation process of a liquid droplet impinging onto a hot substrate. *Int J Heat Mass Transf* 50:303. <https://doi.org/10.1016/j.ijheatmasstransfer.2006.06.012>
 20. Deen N, Kuipers J (2013) Direct numerical simulation of wall-to-liquid heat transfer in dispersed gas-liquid two-phase flow using a volume of fluid approach. *Chem Eng Sci* 102:268. <https://doi.org/10.1016/j.ces.2013.08.025>
 21. Kim DG, Jeon CH, Park IS (2017) Comparison of numerical phase-change models through Stefan vaporizing problem. *Int Commun Heat Mass Transf* 87:228. <https://doi.org/10.1016/j.icheatmasstransfer.2017.07.013>
 22. Hirt CW, Nichols BD (1981) Volume of fluid (VOF) method for the dynamics of free boundaries. *J Comput Phys* 39:201. [https://doi.org/10.1016/0021-9991\(81\)90145-5](https://doi.org/10.1016/0021-9991(81)90145-5)
 23. Wachem BGM, Schouten JC (2002) Experimental validation of 3-D Lagrangian VOF model: bubble shape and rise velocity. *AIChE J* 48:253. <https://doi.org/10.1002/aic.690481205>
 24. Liu XD, Fedkiw R, Kang M (2000) A boundary condition capturing method for Poisson's equation on irregular domains. *J Comput Phys* 160:151. <https://doi.org/10.1006/jcph.2000.6444>
 25. Chorin AJ (1968) Numerical solution of the Navier–Stokes equations. *Math Comput* 22:745. <https://doi.org/10.1090/s0025-5718-1968-0242392-2>
 26. Centrella JM, Wilson JR (1984) Planar numerical cosmology. II—the difference equations and numerical tests. *Astrophys J Suppl Ser* 54:229. <https://doi.org/10.1086/190927>
 27. Scriven LE (1959) On the dynamics of phase change. *Chem Eng Sci* 10:1. [https://doi.org/10.1016/0009-2509\(96\)81820-3](https://doi.org/10.1016/0009-2509(96)81820-3)
 28. Kamei S, Hirata M (1990) Condensing phenomena of a single vapor bubble into subcooled water. *Exp Heat Transf* 3:173. <https://doi.org/10.1080/08916159008946385>
 29. Yang Y, Pan LM, Xu JJ (2014) Effects of microgravity on Marangoni convection and growth characteristic of a single bubble. *Acta Astronaut* 100:129. <https://doi.org/10.1016/j.actastro.2014.04.005>
 30. Sharp DH (1984) An overview of Rayleigh–Taylor instability. *Physica* 12:3. [https://doi.org/10.1016/0167-2789\(84\)90510-4](https://doi.org/10.1016/0167-2789(84)90510-4)
 31. Sidharth GS, Candler GV, Dimotakis P (1991) Baroclinic torque and implications for subgrid-scale modeling. In: 7th AIAA theoretical fluid mechanics conference, pp 1–13. <https://doi.org/10.2514/6.2014-3214>
 32. Roberts MS, Jacobs JW (2016) The effects of forced small-wavelength, finite-bandwidth initial perturbations and miscibility on the turbulent Rayleigh–Taylor instability. *J Fluid Mech* 787:50. <https://doi.org/10.1017/jfm.2015.599>
 33. Tryggvason G (1988) Numerical simulations of the Rayleigh–Taylor instability. *J Comput Phys* 75:253. [https://doi.org/10.1016/0021-9991\(88\)90112-X](https://doi.org/10.1016/0021-9991(88)90112-X)
 34. Berenson PJ (1961) Film boiling heat transfer from a horizontal surface. *J Heat Transf* 83:351. <https://doi.org/10.1115/1.3682280>
- Publisher's Note** Springer Nature remains neutral with regard to jurisdictional claims in published maps and institutional affiliations.